EXPERIMENTAL AND NUMERICAL INVESTIGATION OF HELICOPTER FUSELAGE MODEL WITH ACTIVE FLOW CONTROL.

Fabrizio De Gregorio and Pier Luigi Vitagliano

Fluid Mechanics Department, Italian Aerospace Research Centre (CIRA)
Via Maiorise, 81043 Capua, Italy

Keywords: **Bluff body, Active Flow Control, Pressure Drag, PIV, CFD, U-RANS**.

Abstract

Scope of the work was investigating both experimentally and numerically the flow characteristics in the wake region of a simplified helicopter fuselage model featuring a rear ramp. A dedicated wind tunnel test campaign was carried out, including surface pressure and flow field measurements. The possibility to decrease the pressure drag and to improve the aerodynamic performance was investigated using two types of active flow control (AFC) systems: a “steady jet” actuator and a “pulsed jet” actuator, blowing from three slots located near the edges of the loading ramp. Several AFC operating configurations were tested by changing the blowing coefficient at the three slots and the pulsed jet reduced frequency. Useful information and deeper understanding of the flow behavior was obtained for a future test campaign scheduled on larger scale in an industrial wind tunnel. The results indicated that one operating condition was definitely more efficient than the others. Threshold values were observed in the functioning of the AFC actuators. In parallel the aerodynamic behavior of the fuselage model have been investigated by CFD simulations, with the objective to demonstrate the capabilities and limitations of currently available unsteady flow solvers to reproduce the flow features and the wake modifications induced by flow control, and the perspective to design better flow control techniques and model shapes. The paper reports the experimental set-up, the steady and pulsed jet flow control systems, the CFD methodology, a selection of the gathered results, comparisons between experimental and numerical results and perspective of the futures activities.

1. INTRODUCTION

The performance of heavy transport helicopters, having a large, and almost flat, aft loading ramp suffer from the poor aerodynamics of the aft body. For helicopters in cruise flight condition, the component of the rotor power due to counter balance the parasite force was of the order of 40% to 55% of the total requirements, as stated by Gatard et al in 1997[1]. Nowadays fuselage and rotor head drag breakdown studies[2]-[3] indicate that about the 70% of the total drag can be ascribe to the fuselage and the remaining 30% is due to the rotor head, a further fuselage drag breakdown indicates that the cabin contributes with about 60%, tail, sponson, and exhaust respectively for about 16%, 14% and 10%. Consequently in order to improve the helicopter speed, range, capability, stability and reduce the fuel consumption and the environmental impact, the fuselage drag reduction is one of the main objectives of the industrial designers. The presence of the aft door (or “loading ramp” as it often referred to) dictates flat and inclined surface connected to the fuselage at almost its widest cross section. This, in turn, causes flow separation at the lower corner, generating a bubble and a system of streamwise vortices at the sides. These vortical structures present some similarity to those separated from hatch-back cars[4]. The flow separation and the longitudinal vortex always cohabit on the aft region, when the flow separation is predominant the flow is named “eddy flow”, when the flow separation is reduced and the longitudinal vortices are predominant the flow is called “vortex flow.”

Both flow typologies provide an important contribution to the fuselage drag-form. Together with the increment of the pressure drag the flow separation interacts with the fuselage tail structures inducing strong vibration and submitting the airframe to fatigue cycles. The fuselage drag depends by the fuselage incidence angle (α) and by the loading door upsweep angle (ϕ) as investigated by Seddon in 1990 [5] and well described in the diagram presented in Figure 1, where the drag coefficient behaviour is presented versus the upsweep angle for different fuselage attitudes. For fixed upsweep angle, an abrupt increment of the pressure drag occurs passing from eddy flow to vortex flow. This aspect must be taken into account designing the flow control

system, not always the suppression of the flow separation induces a reduction of the pressure drag, in the case that the longitudinal vortices come closer to the fuselage surface the induced negative pressure produce an increment of the drag as well as of the lift download.

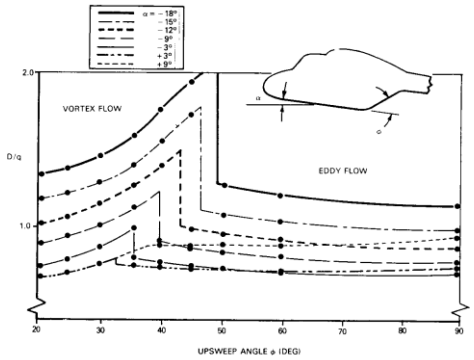

Figure 1: Variation of drag with upsweep angle at constant incidence (Seddon 1990).

Seddon also provided a summary diagram of the flow topology (Figure 2) for a wide range of incidence angles and upsweep values. The knowledge of the flow characteristics on rear loading ramp is the first step for designing a flow control system able to reduce the fuselage drag not at detriment of the lift.

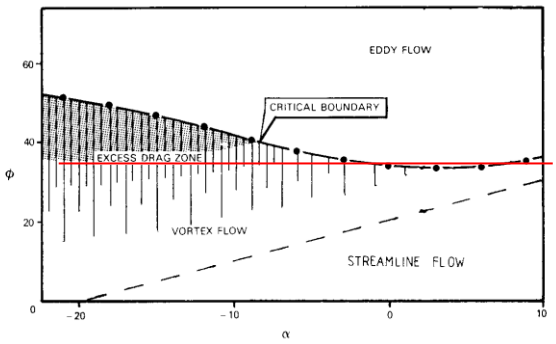

Figure 2: α–ϕ diagram showing all type of flow and indicating excess drag region (Seddon 1990).

Seddon proposed some passive control systems for reducing the drag-form, ones was to install several deflectors on the fuselage side immediately ahead of the upsweep face in order to prevent the formation of vortex flow. Later industrial tests indicated that deflectors, strakes or ridges alleviates the vortex flows but incremented the fuselage drag. Recently vortex generators systems are investigated in order to reduce the fuselage drag, Boniface[6] claimed a reduction of about 5% for zero attitude angle and a reduction between 1.5 to 5.5% varying the incidence angle in the range between -12° to +8° by performing a CFD investigation of the GOAHEAD-like[7] fuselage. During the last years the research in the field of the active flow control (AFC) actuators drawn large interest in the aeronautical field, one of this actuators was the zero-net-mass-blowing actuator (or synthetic jet). In 2005 Martin et al[8] investigated numerically and experimentally the influence of 12 SJ actuators on a helicopter fuselage obtaining drag reduction in the range between 6 and 10% and an impressive reduction of the lift download of a value of 40%. Martin also investigated the influence of the position of the SJ slot on the fuselage, claiming that for eddy flow the SJ located on the bottom of the upsweep ramp were more effective whereas for vortex flow the main contribution to the drag reduction was obtained by the fuselage side slots. Analogous results were obtained by Ben-Hamau in 2007 obtaining similar drag reductions in the range between 3 to 11% for different attitudes[9]. In 2010 a NASA and ONERA[10] collaboration investigated numerically and experimentally the behaviour of different AFC systems (steady blowing, pulsed Jet and SJ), obtaining remarkable result in drag reduction, with the steady blowing system able to reduce up to 35% the fuselage drag but requiring pressurised air and the zero-net-mass-flux actuator inducing a decrement up to 26%. A contribution to understand the ACF influence on the helicopter fuselage has been provided by Lienard et al[11] and Le Pape et al[12] with their comprehensive work investigating the effect on the fuselage drag and lift download. A further promising control system is the COMPACT (Combustion Powered actuation)[13] a novel technology which exploits the chemical energy of gaseous fuel/oxidizer mixture to create a high pressure burst and subsequent high momentum jet of exhaust products. In 2011 the chemical powered actuators[14]-[15] were investigated on a ROBIN fuselage model obtaining a drag reduction of the order of 12 to 17 % but also a significant increment of the lift download. Another interesting actuator is the fluid oscillators investigated by Martin et al[16] on the ROBIN fuselage equipped of powered rotor. The results indicated, in some cases, a reduction of the total drag of the order of the 20% respect the baseline configuration. Although many effort have been performed in the past, still large interest is existing nowadays and different flow control systems are investigated in order to increase the fuselage performance and additional effort are necessary in order to understand the interaction between the flow topologies and the selected actuators.

This work aims to investigate the flow characteristics of a typical helicopter transport fuselage and the possible benefit in terms of drag reduction by using

steady and pulsed jet blowing flow control systems. The research has been carried out in the framework of the fuselage drag reduction task of the Green Rotorcraft ITD of the Clean Sky Project founded by the European Union. The task combined CFD and experimental activities for jointly investigate the phenomena. The project foresaw to investigate the performance of the steady and pulsed blowing jet at laboratory level on a limited size helicopter model for successively considering the effect on a larger fuselage model scale (1:7 of the AW101 transport helicopter). A devoted unsteady blowing system, based on a rotating valve was designed, built and characterised in terms of mass flow, mean and instantaneous velocity, pulse frequency. This work presents part of the comprehensive experimental test campaign carried out at CIRA CT-1 wind tunnel on the small helicopter fuselage model at Reynolds number of 1 million and the preliminary CFD results. The paper describes the experimental set-up, the flow control actuator, the simplified fuselage model together with the CFD methodology. The performed test matrix is discussed together with the results obtained by the experimental and CFD simulation of the clean fuselage baseline and the effect of the different AFCs for the different selected configurations.

2. EXPERIMENTAL LAY-OUT

2.1. Model and Instrumentation Description

The investigation was carried out on a simplified helicopter fuselage model of the AW101 transport helicopter with an upsweep angle of ϕ=35°. The fuselage model was characterized by the following main sizes: length of 422.5 mm, height of 70 mm and width of 70 mm. The model was instrumented with 64 pressure taps located on the model centreline, on the region of the rear hatch and of the tail boom (Figure 3). The pressure taps were connected to two ZOC22/32px differential pressure transducers with full scale (FS) value of 1 psi (6894 Pa) and accuracy of 0.12% of Full Scale. For each different test condition the mean pressure values were recorded. The estimated accuracy for the pressure coefficient is equal to 0.011. The location of the pressure taps was limited by the internal pneumatic route of the AFC system.

2.2. Wind tunnel description

The test campaign was conducted at CIRA CT-1, an Eifel type open low speed tunnel. Test section main sizes are: height of 305 mm, width of 305 mm and length equal to 605mm. Maximum achievable flow speed is 55 m/s with a turbulence level of 0.1%. The full test campaign was carried out at constant speed of V_∞=34 m/s and Reynolds number, based on the fuselage length, of $9.9*10^5$. The model has been investigated varying the fuselage incidence angle in the range between -11° to +11° with step of 2.75° plus an additional angle at α=-1.5°. The blockage ratio was between 5.3 to 6.1 % respectively for α=0 and α=±11° inducing some wall interference effect to be taken into account. The model was mounted up-side down in order to avoid any disturb on the ramp region coming from the ventral support.

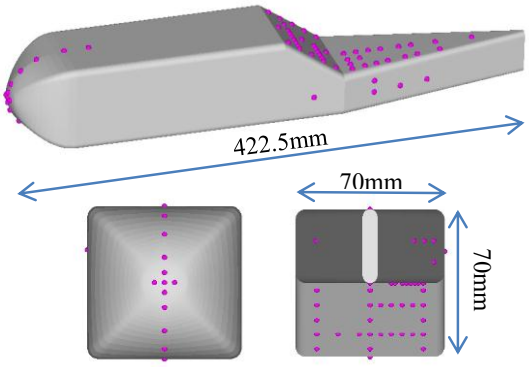

Figure 3: PTS locations on the model

2.3. Flow control system description

The simplified fuselage model was designed in order to locate three actuator slots in the loading ramp region, in particularly, the slot 1 on the bottom of the loading hatch and the slot 2 and 3 on the ramp sides as shown in Figure 4.

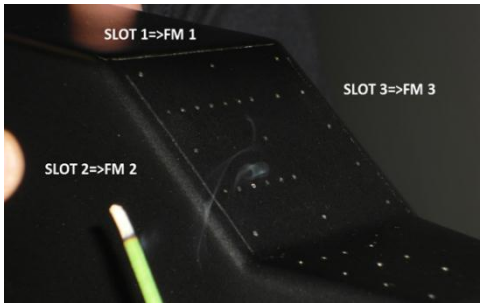

Figure 4: Detail of the loading ramp showed up-side down

Each slot was connected to a dedicated pneumatic circuit feed by pressurized air. Up-stream each slot a resonant cavity was present in order to level the flow coming out from the slots. The slots were characterised by the same jet axis angle inclined respect the ramp surface of α_j=45° and by the same slot thickness equal to 0.5mm. The slot lengths were slightly different, slot 1 was equal to L_{S1}=63.5mm whereas slot 2 and 3 lengths were L_{S2}= L_{S3}=54.7mm.

Two different AFC systems were considered: *steady jet* and *pulsed jet* blowing from the rear slots. The *steady blowing* jet was obtained by a steady pressurized air feeding the cavity.

The *pulsed jet* was obtained through a steady air supply modulated by rotating valve (Figure 5) inducing unsteady excitation that was transmitted to the actuator (cavity) by a pneumatic line. The rotating pneumatic valve consists of two concentric cylinders. The inner cylinder (or rotor) rotates around its axis of revolution driven by an electrical stepper motor. The Outer cylinder (or stator) is fixed. The inner cylinder contained 11 apertures with diamond shape and equally angular spaced ($\Delta\varphi$=32.72°) on the same circumference. The outer cylinder contains 6 circular apertures along the circumference and in correspondence of the rotor apertures. The air transfer is obtained when the rotor apertures aligns with the stator apertures. The pulse frequency f_j is calculated multiplying the rotating speed by the number of rotor apertures $f_j=\omega*N_s$.

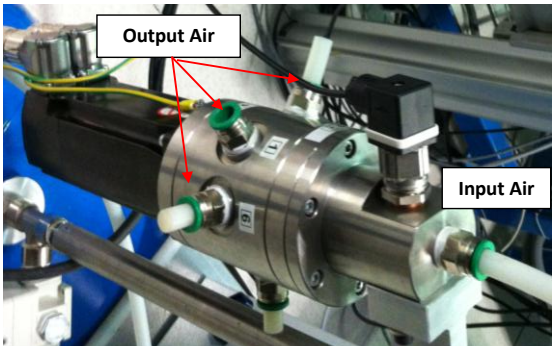

Figure 5: Pneumatics rotating valve.

Before the wind tunnel test campaign, particular care was taken for characterising the steady and pulsed jet pneumatic system. A dedicated laboratory test campaign was aimed to obtain the transfer function relating the flow volume rate to the mean and maximum jet velocity for each single slot. For the pulsed jet system the velocity time history was measured varying the pulsed frequency and the volume flow rate. Once that the steady and pulsed jet were characterized in term of mean and peak velocity and achievable frequency range it was possible to calculate the characteristic non dimensional quantities defined for evaluate the flow control system. In particular the pulse jet frequency normalised as:

$$F^{+}=f_j \cdot W/V_\infty$$

where f_j is the pulse jet frequency, W the fuselage width and V_∞ the free stream velocity and the blowing coefficient, defined as the sum of the contribution of each blowing jet:

$$c_\mu = \frac{\sum_j \rho_j A_j V_J^2}{A_{CS} 0.5 \rho_\infty V_\infty^2}$$

where A_j, ρ_j and V_j are respectively the actuator slot surface, flow density and maximum speed and Acs , ρ_∞ and V_∞ are the fuselage cross section, free stream density and velocity. The detailed description of the ACF systems and of the jet exit characterization is given in the reference [17].

2.4. **Flow characterization**

In order to characterise the flow topology on the loading ramp region stereo PIV measurements have been performed. The flow behaviour in proximity of the model bottom surface was investigated along the full model length on three parallel longitudinal planes (y/(W/2) =0; 0.29 and 0.60) using two components PIV measurements and by three components Stereo PIV measurements on several cross parallel planes starting immediately downstream the loading ramp (x/L=0.58, 0.63, 0.68, 0.72, 0.75, 0.77). The PIV system was composed by two Nd-Yag resonator heads providing a laser beam of about 250 mJ each at 532 nm and by two double frame CCD cameras (2048x2048 px). Particles of about 1 μm of diameter, composed by DEHS oil, were used as seeding. The laser sheet was delivered from above in the measurement region. For the longitudinal planes measurements, the camera was located on the left side of the test section mounted on 2D traversing system in order to cover the full length of the model. Different focal length lens were used for varying the flow field space resolution. The PIV data resolution ranges from 1.1 to 0.6 vectors per millimetre for Field of View sizes ranging from 140x140mm^2 to 80x80mm^2. The cross plane investigation foresaw stereo PIV measurements. The cameras were equipped by motorised Scheimpflug systems and located on both sides of the test chamber. Each Camera was mounted on 2D linear traversing system (Figure 6). The laser lens was installed on a linear traversing system in order to automatically traverse the region of interest synchronizing with the camera positions. The cameras aimed to the cross pane with and angle of about 45°. For the cross plane measurements the spatial resolution obtained was equal to 1.1 vector for millimetre for a field of view of 150x100mm^2. Ensemble average and RMS values

were calculated for each test condition on a data sample of 150 velocity maps.

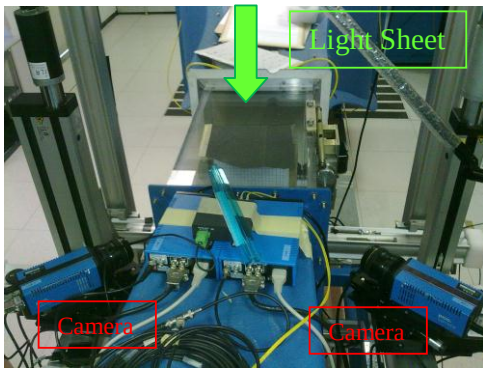

Figure 6: Stereo PIV experimental lay-out

3. CFD METHODOLOGY

Despite large progresses achieved in past years by CFD and the large improvement in computer speed, simulation of separated flows is still a challenge, not only for the lack of reliable theoretical models, but also because of the computational effort required, concerning unsteadiness and instability. In our simple model the flow shows already a quite complex behaviour by changing the angle of incidence, flow control introduced by steady and unsteady blowing with different strategies from three slots located at the beginning of the rear ramp strongly affects the wake development. Main objective of this work is to demonstrate the capabilities and limitations of currently available unsteady flow solvers to reproduce the flow features and the wake modifications induced by flow control, with the perspective to predict and design different (and better) flow control techniques and model shapes. As the unsteady flow is not periodic, questions rise about the validity of U-RANS model for such simulations. Results shown in this paper have been computed using a compressible U-RANS model, with k-ω TNT turbulence model[19]. No significant differences with respect to other models, like k-ω SST[18] and Spalart-Almaras[20] have been noticed in a few test cases that were carried out for comparison.

The flow solver U-ZEN[21] is based upon structured multi-block meshes, cell-centered, finite volumes central spatial schemes with artificial dissipation. Time derivatives are discretized with a three level implicit scheme, integration is performed with dual time stepping technique[22] by using an explicit 5 stages Runge-Kutta scheme and a linear prediction formula at the first step. Since our simulations are performed at low Mach number, preconditioning is applied in the dual time iterations, which effect is not only to accelerate convergence, but also to improve accuracy[23][24].

Domain shapes include the wind tunnel walls and fuselage model without the vertical pylon. Flow is simulated without symmetry conditions in the central section, in order to allow for flow instabilities to develop in the cross-plane direction. Computational mesh is made of 60 blocks with about 12 million cells. About 350 cells are located in longitudinal direction along the fuselage, with 128 on the rear ramp only, 320 cells in circumferential direction and 104 in normal direction (see Figure 7).

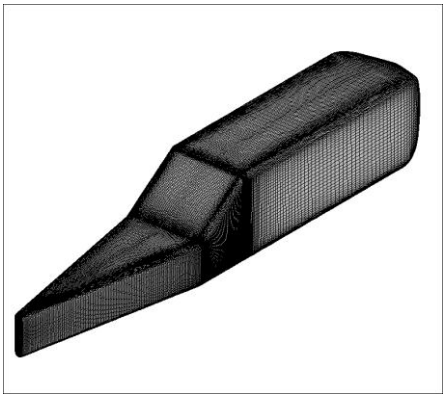

Figure 7: Surface mesh. Wind tunnel Walls not shown

The three slots contain 16 cells across the thickness. Inflow through the slots (when activated) is simulated by fixing momentum and density, while pressure is extrapolated from inside the flow field. No slip adiabatic wall conditions are assigned on the fuselage, free slip adiabatic conditions on the wind tunnel walls. Tests carried out with different meshes show no significant differences in the results on the lower ramp when the pylon is modeled and the wind tunnel wall boundary layer is simulated. Free stream boundary conditions are applied at the channel inlet, pressure is fixed at the exit, with other variables extrapolated from inside.

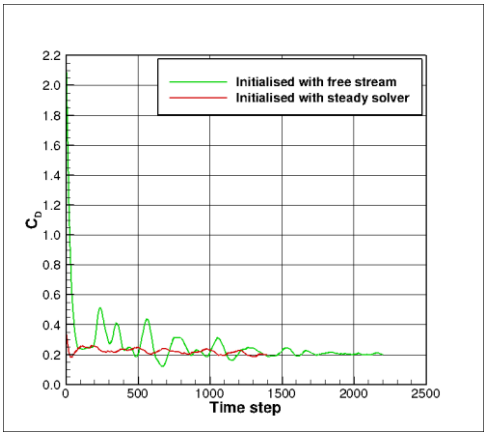

Figure 8: Time history of drag coefficient for test case α=0 without flow control.

Computations are carried out with time step of 37 μs; 1500-2000 time steps are required to obtain a reasonably converged solution (**Figure 8**), which corresponds to the time the free stream crossing about 6 times the model length. Flow variables are then averaged over at least 500 time steps for post-processing.

4. TEST MATRIX

The test matrix has foreseen first the investigation of the aerodynamic behaviour of the baseline model without AFC system in order to characterise the flow characteristics in loading ramp region varying the angle of attack. The model incidence angle was varied in the range between -11° to +11° with a step of 2.75° and with a further intermediate position at α=-1.5°. Once that the baseline behaviour was assessed, the influence of the steady and pulsed jet was investigated varying the flow control parameters for all the selected incidence angles in the operating range reported in Table 1.

Parameters	Range
Reduced Frequency < F^+>	0.15 – 1.13
Blowing momentum coefficient <$c\mu$>	0.02 – 0.1
Number of slots	3
Operating configurations	Single slot, Side slots, All slots,

Table 1: AFC parameters

Three different operating conditions were applied (Figure 9):

a. Single bottom slot blowing,
b. Side slots blowing,
c. All slots blowing.

The first test campaign was aimed to measure the model pressure distribution and detected the values of reduced frequency and blowing coefficient for which the surface pressure indicated a flow reattachment and an alleviation of the pressure drag. In a second time the flow field measurements were performed on a limited number of selected test conditions.

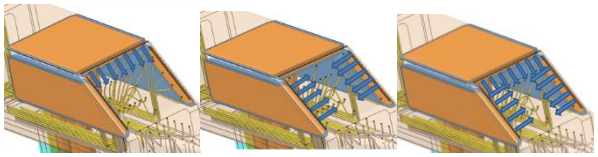

Figure 9: AFC operating configurations: a) Single slot blowing, b) Side slots blowing and c) All slot blowing.

Computations have been carried out without flow control at angles of attack α ranging from -11° to 11° degrees, to cover the experimental test matrix. Concerning the steady blowing conditions, after preliminary experimental results it was decided to investigate five angles of attack (α=-11°,-5.5°, -2.75°, 0°, 5.5°), with the three operating conditions and two different blowing coefficients. The idea was to simulate the conditions just before the full saturation, which apparently occurs when outflow velocity overcomes the free stream velocity. Only preliminary results for a limited amount of test cases are discussed in the present report, since not all the simulations were completed.

5. RESULTS

5.1. Baseline

The baseline model configuration was investigated by surface pressure and velocity field measurement. The results clearly indicated that the flow in the region of the loading ramp can be considered as eddy flow being characterized by a marked flow separation in the range from α=+11° down to α=-2.75°. For α=-5.5° the vortex flow starts to be predominant, for becoming predominant for lower attitudes. This behavior is clearly detectable from the pressure longitudinal distribution of the lower model surface.

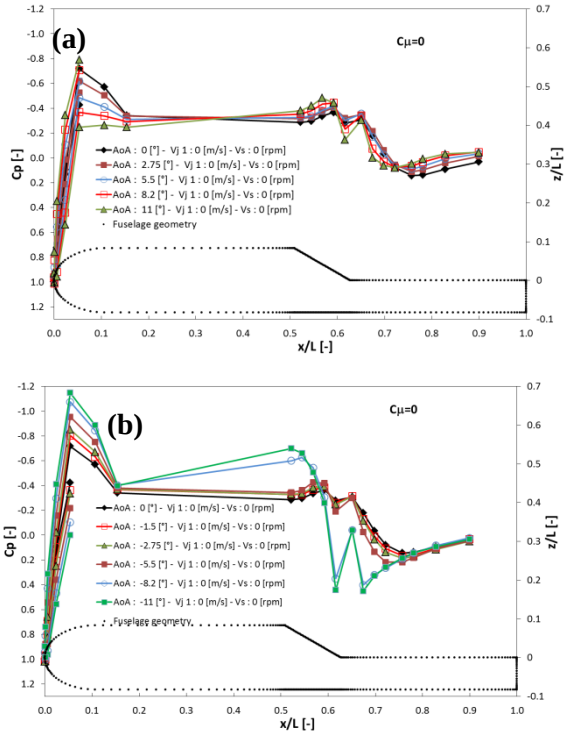

Figure 10: Centreline pressure distribution varying the incidence angle

The results indicates that for all the positive values of

the model attitude the pressure distribution presents a plateau in correspondence of the ramp flow separation for recovering only downstream on the tail cone (**Figure 10**a) with marginal changes due to the model angle variation in the ramp region. Whereas starting from α=-5.5° the flow separation starts to reduce and the pressure becomes recovering on the loading ramp (Figure 10b). As already said, the Eddy and Vortex flow phenomena always cohabitate, so it is not easy to define a clear the transition point.

We can state that the transition from eddy flow to vortex flow can be pointed out for model attitude between -2.75° and -5.5°. Confirmation of the flow behavior was provided by the stereo PIV results obtained on the cross flow measurements planes equal space located starting from the loading ramp and moving downward along the tail cone. Immediately downstream the end of the loading ramp (x/L=0.675), the mean velocity fields (Figure 11) presents for an incidence angle of α=0° a flow separation happening on the fuselage bottom surface. Flow separation that decreases as the model attitude angle moves toward negative values. At the same time while the flow reattachment is taking place a clear couple of contra rotating vortices appears on the edge of the flow separation region for later positioning on the fuselage surface as the reattachment occurs.

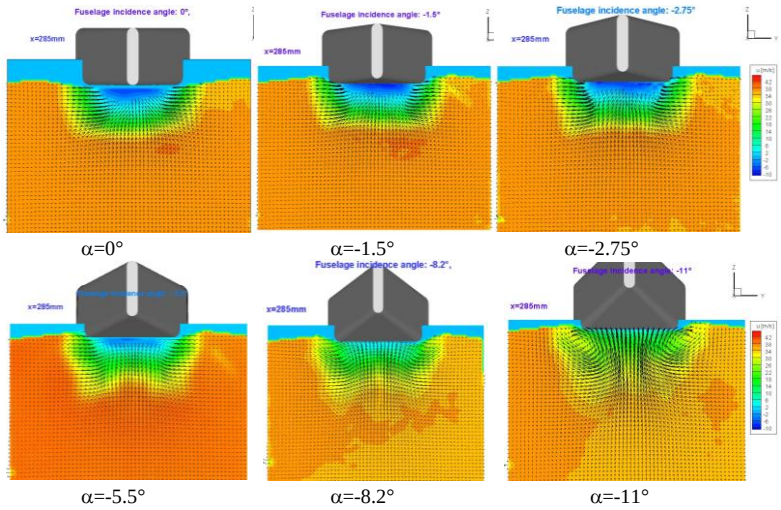

Figure 11: PIV Cross-flow velocity vector field with out of plane colour map varying AoA (x/L=0.675)

5.2. **Experimental/Numerical comparison**

Hereinafter the flow characteristics of the model baseline are discussed together with the assessment of the preliminary CFD results. For the test case of α=0° the CFD results reached 2200 time step. The mean values have been obtained averaging on the last 500 steps in order to compare with the mean experimental data. The longitudinal pressure distribution presents a good agreement with the measured pressure coefficient (**Figure 12**). The CFD results are able to detect also the pressure drop occurring due to a secondary recirculation bubble on the junction between the ramp and the cone tail but slightly overestimate the pressure recovery on the tail cone. The pressure coefficient (Cp) spanwise distribution also presents a good agreement with the PTS data in correspondence of the ramp, but again overestimates the pressure recovery on cone tail at x/L=0.675 (Figure 13). In order to facilitate the reading of the pressure comparison the label of the pressure taps on the rear model region are described in Figure 14.

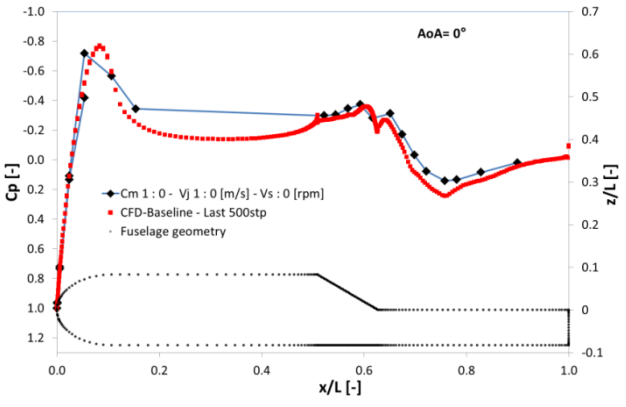

Figure 12: EXP and CFD Cp comparison along the model centreline for α=0°

To confirm this results the longitudinal flow velocity behaviour at the three different planes are compared (Figure 15). The PIV data in agreement with the pressure taps presents a clear flow separation on the

loading ramp for downward reattaching to the fuselage at about the x/L=0.7. The flow velocity measured on the cross flow planes clearly indicates as for α=0° a condition of eddy flow occurs (Figure 16). The same figures presents the velocity vector maps obtained by the numerical simulation.

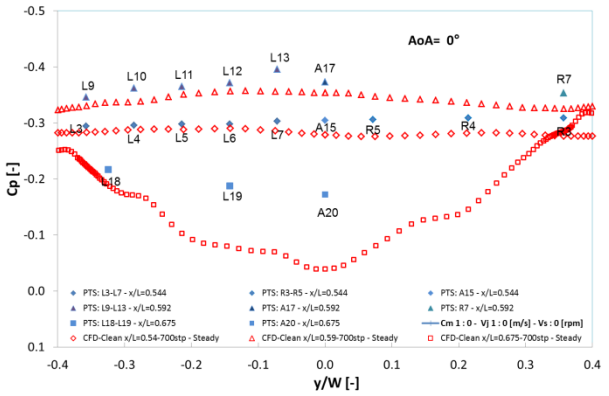

Figure 13: EXP and CFD Ramp spanwise pressure distribution for α=0°

The visual comparison present a fairly good agreement with the PIV data both on the longitudinal planes as well as on the cross plane. The flow topology and quantitative results indicates the capability to reproduce the flow characteristics. The main difference with the experimental data is a delay in the flow reattachment (Figure 24).The diagram compares the flow reattachment locations measured by the PIV longitudinal plane as the point where the inversion of the tangential velocity measured on the model surface occurs (diamond blue marker) with the CFD blue line obtained by the tangential skin friction distribution (Figure 23 a).

The CFD flow reattachment is defined as the line where the longitudinal component of the skin friction change sign, in the figure is the border of the black region.

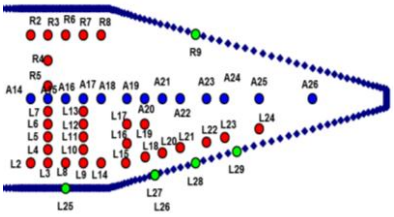

Figure 14: PTS location on the model ramp and tail cone

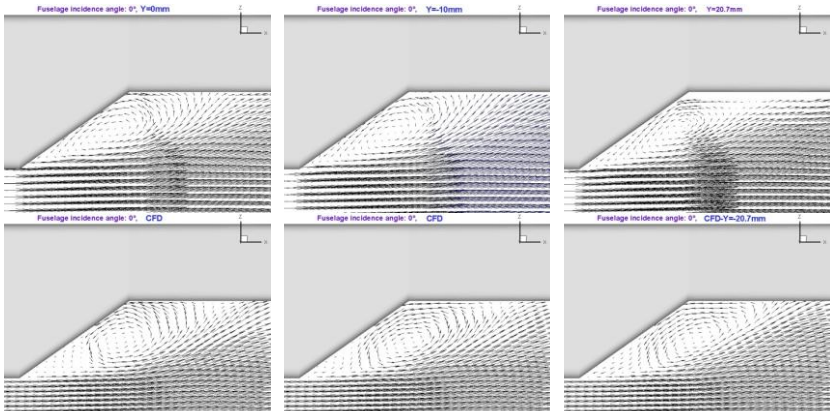

y/(W/2)=0 **y/(W/2)=0.29** **y/(W/2)=0.60**

Figure 15: PIV-CFD longitudinal flow velocity at α=0°

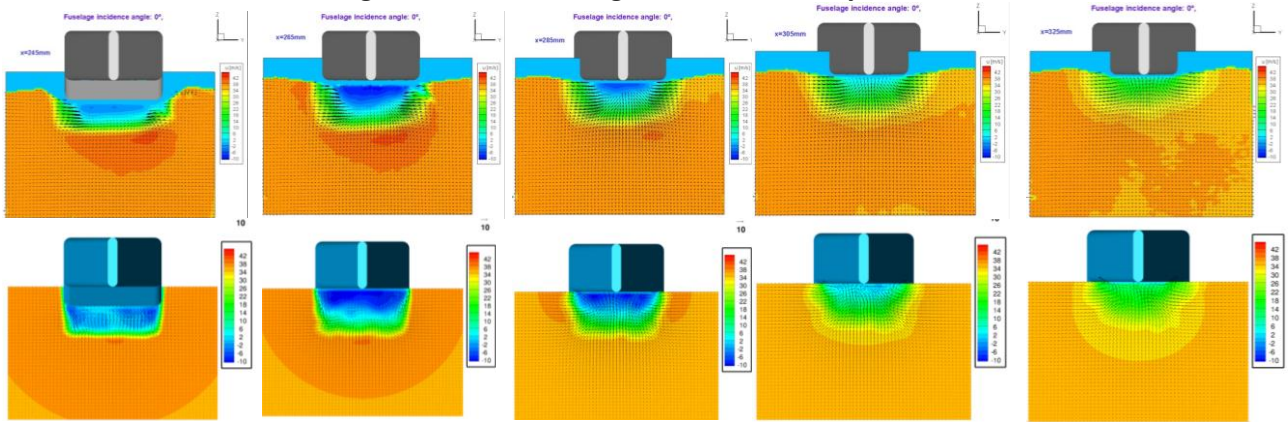

x/L=0.58 **x/L=0.63** **x/L=0.67** **x/L=0.72** **x/L=0.77**

Figure 16: PIV and CFD cross plane velocity map comparison for α=0° (PIV upper row and CFD lower row).

For α=-5.5°, the CFD reach the number of 1300 steps, so that the mean data have been obtained on the average of the last 500 steps. The comparison with the experimental pressure data indicates a large discrepancy (Figure 17).

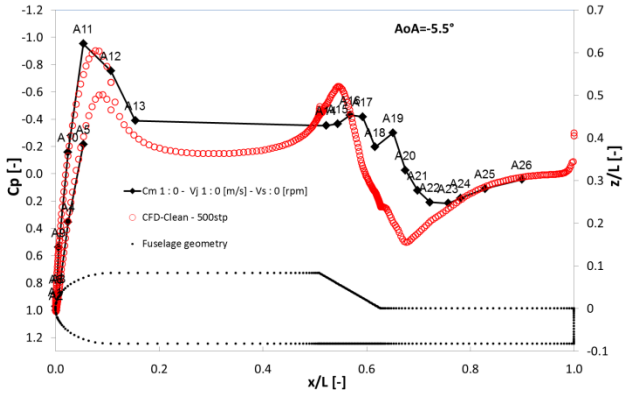

Figure 17: EXP and CFD Cp comparison along the model centreline for α=-5.5°.

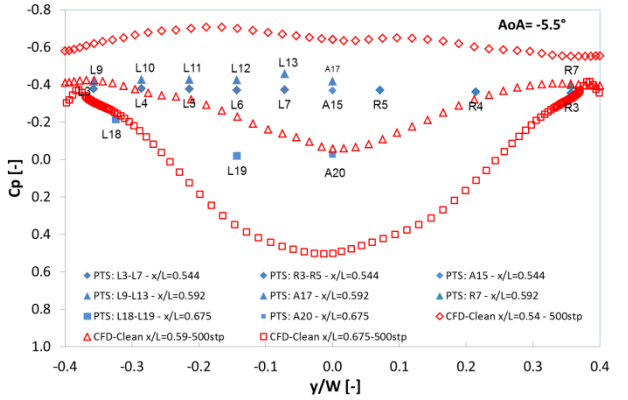

Figure 18: EXP and CFD Ramp pressure distribution for α=-5.5°.

The pressure coefficient distribution along the model centreline presents a slight under estimation on the suction peak in proximity of the fuselage nose, followed by a marked over estimation of the suction peak on the beginning of the ramp for later overestimating the pressure recovery on the cone tail and anticipating the minimum peak. The agreement between the CFD and WT data occurs downstream x/L= 0.77. Analogous also the spanwise pressure distribution presents noticeable differences (Figure 18). As expected after 1300 time step the convergent was not reached yet.

For α=-8.2°, although the code reached only 700 time steps, the agreement with the experimental data was better of the case previous case. The longitudinal pressure distribution again presents smaller values respect the expansion peak in proximity of the nose but the beginning of the loading ramp is characterized by a remarkable agreement, followed by a smaller over pressure recovery and by a good agreement on the tail cone (Figure 19). In this case unlike of results obtained for incidence null the code was not able to detect the expansion peak at the end of the ramp. The Cp spanwise distribution on the model ramp and tail cone presents similar behavior on the beginning of the ramp but quantitative shifted toward larger value and same qualitative and quantitative results on the tail cone.

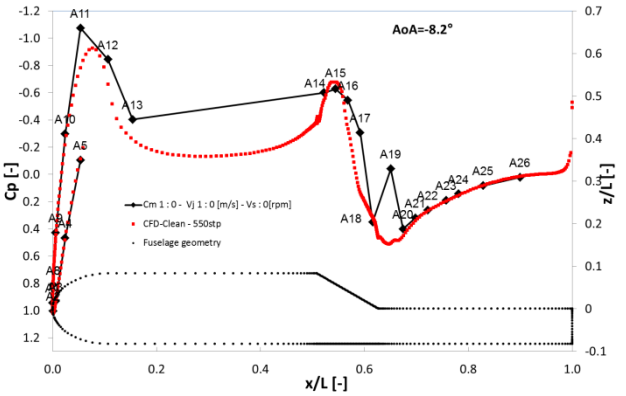

Figure 19: EXP and CFD Cp comparison along the model centreline for α=-8.2°.

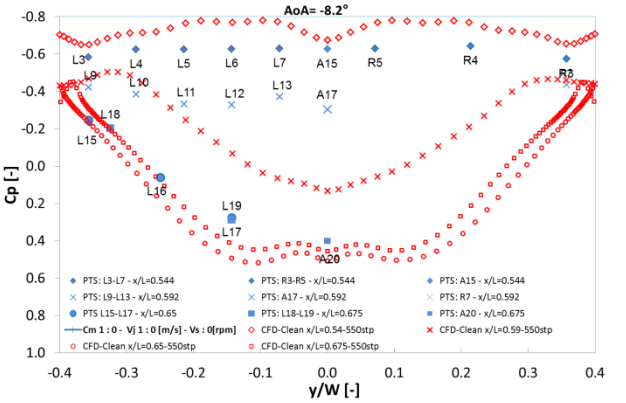

Figure 20: EXP and CFD Ramp spanwise pressure distribution for α=-8.2°.

The data presents a mismatch in the middle of the ramp where the CFD presents a large flow reattachment respect the experimental data (Figure 20). The comparison is carried out also on the longitudinal flow velocity planes (Figure 21). The vector plots present a remarkable agreement between the CFD and the PIV data. The PIV data presents a small recirculation bubble covering the full loading ramp in the center line for decreasing moving toward the model side. Let note that at y/W=0.60, the flow presents a first separation bubble at the beginning of the ramp followed by a second smaller bubble to the end. The CFD vector plot presents a notable agreement except that for a smaller under estimation of the flow separation as visible in the cross plane velocity fields (Figure 22). The PIV data shows on the ramp (x/L=0.58) a smaller flow separation along the full model spanwise while the CFD vector field present a smaller flow separation

confined close the centerline. Similar behavior is observed at the end of the ramp (x/L=0.63). Moving downward the fuselage length a clear vortex flow is measured and simulated. Analogous to the α=0°case, the flow reattachment location has been calculated on the PIV data as well as on the CFD results. The reattachment points have been obtained on the longitudinal velocity field by detecting the tangential velocity inversion point starting from the PIV and CFD data vector plot (respectively full blue triangle marker and empty red triangle marker in Figure 24).

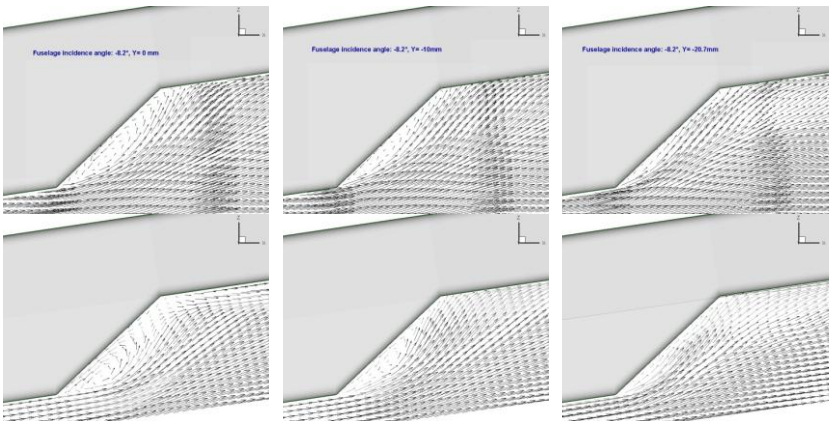

Figure 21: PIV-CFD longitudinal flow velocity at α=-8.2°

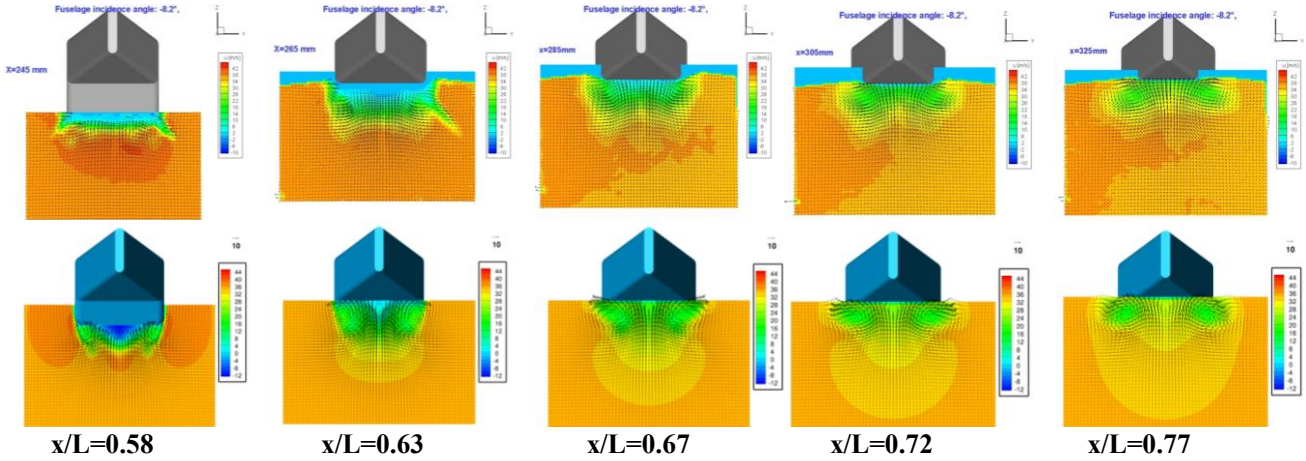

Figure 22: PIV and CFD Cross plane velocity map comparison for α=-8.2° (PIV upper row and CFD lower row).

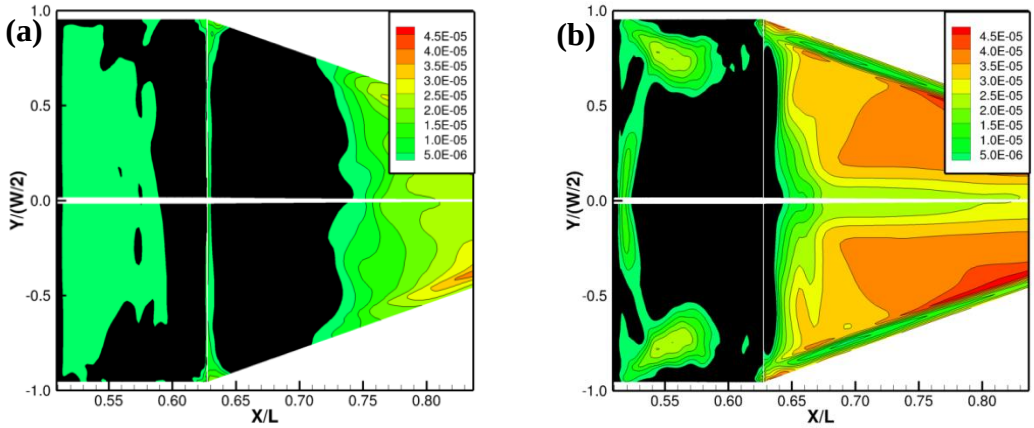

Figure 23: CFD skin friction contour map for α=0° (a) and α=-8.2° (b)

Furthermore the reattachment line is obtained by the skin friction distribution of the fuselage bottom. The separation line is detected as change of sign of the skin friction longitudinal components. In the Figure 23 is indicated by the contour of the black region. The results indicates a good agreement between the

CFDF and PIV data regarding the reattachment points.

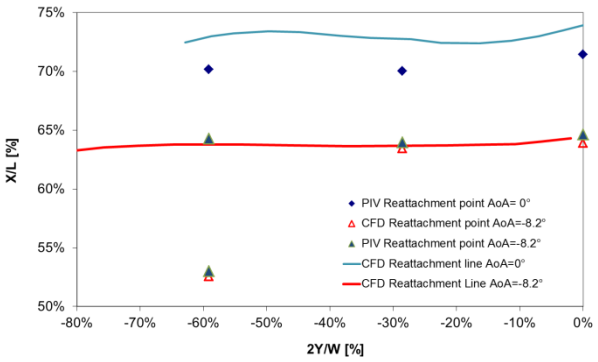

Figure 24: PIV and CFD flow reattachment points.

5.3. **Active Flow Control Results**

The effect of the active flow control is discussed only from the experimental point of view. The CFD solution did not yet converged. The behavior of the steady blowing jet on the pressure distribution was investigated for all the three different operational conditions on a wide range of jet speed and consequently different blowing coefficients C_μ. For all the operational conditions the following similar behavior was observed: increasing the velocity jet, an improvement in terms of pressure recovery was witnessed up a limit value beyond that further jet velocity increment was useless in terms of pressure recovery but a negative suction effect was observed at the bottom of the ramp. This threshold values were detected for all the different incidence angles and for all the different operational conditions. It was found that the velocity threshold value was always comparable with the free stream velocity. As example, the pressure distribution on the model centerline for different values of the jet speed and respectively for a single operating slot, for both side slots blowing and for all the slots operating in contemporaneity are presented in Figure 25 a, b and c. In order to evaluate the most efficient operational condition, the improved pressure distribution was compared for the different configurations. For all angle of attacks, the operating condition characterized by a single slot was the most effective. The configuration with a single slot presented a far better pressure recovery on the ramp on equal terms of jet speed but with smaller values of blowing coefficient: c_μ=0.014 against values of c_μ=0.026 and c_μ=0.029 respectively for side slots and all slots operating Figure 26 .

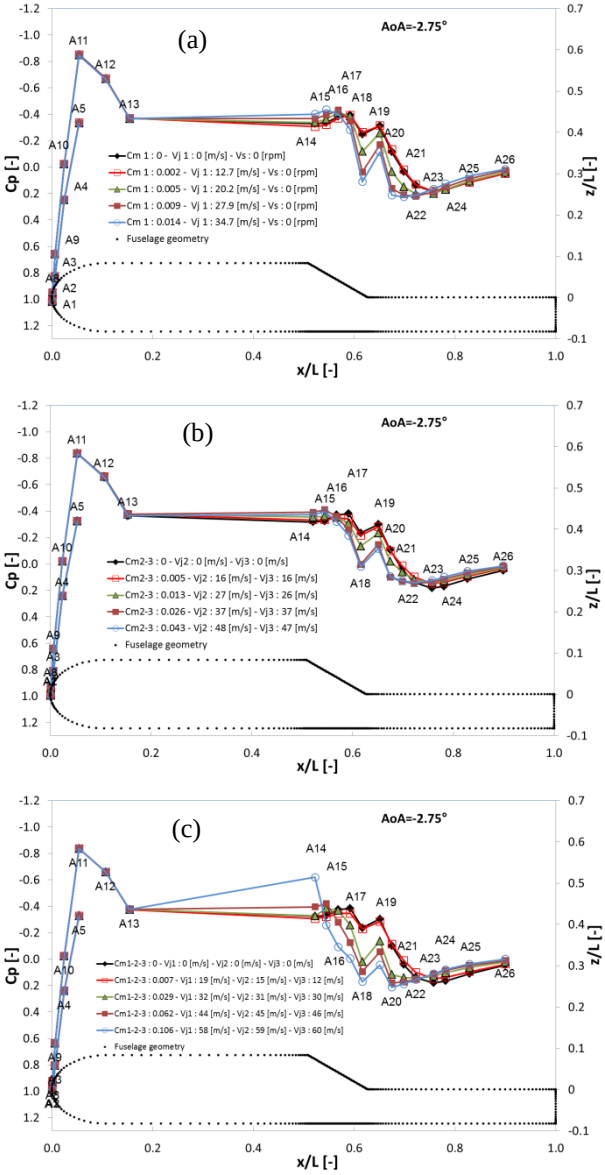

Figure 25: Pressure distribution for α=-2.75° varying the jet speed V_j for single slot blowing (a), side slots blowing (b) and all slot blowing (c).

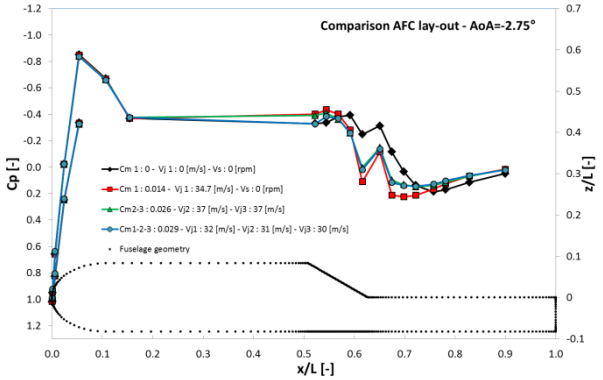

Figure 26: Pressure distribution for α=-2.75° for different operational condition for optimized blowing coefficient.

For further information the influence on the spanwise

pressure distribution is discussed (Figure 27). The pressure coefficient behavior on the lower and rear region of the fuselage model is investigated with and without flow control. The saturation condition for the single slot blowing has been selected. The baseline case (bleu full marker on Figure 27) presents a flat behavior in the ramp region indicating a full separated flow for later slightly recovering on the tail cone. The case with activated flow control system (red empty marker on Figure 27) presents on the first ramp region an increment of the suction peak induced by the blowing jet, followed by a continuous pressure recovering moving backward. The span wise pressure distribution indicates a suction peak on the model sides due to the occurring of the counter rotating vortices.

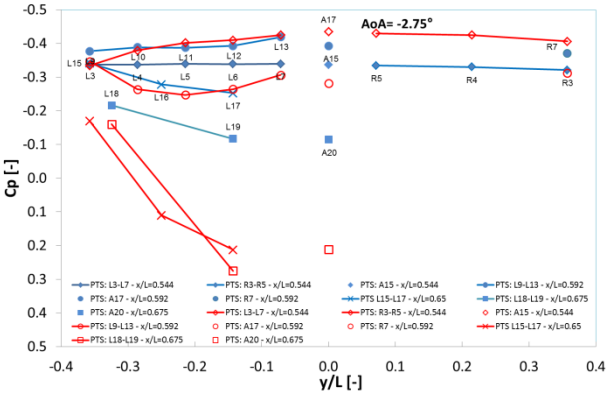

Figure 27: Spanwise Cp distribution with and without flow control (α=-2.75°)

Once that the threshold values were detected the effect of the pulsed jet on the rear loading ramp was investigated varying the jet frequency as well as the mean jet speed. Varying the jet frequency no appreciable variation were observed (Figure 28). This was due to the weak velocity fluctuation provided by the AFC system to the jet slot exit. The long pneumatic circuit reduced the velocity fluctuation and increased the mean velocity cancelling the advantage of a pulsed jet, i.e. the reduced requested of blowing air. The predominant parameter remained the blowing coefficient.

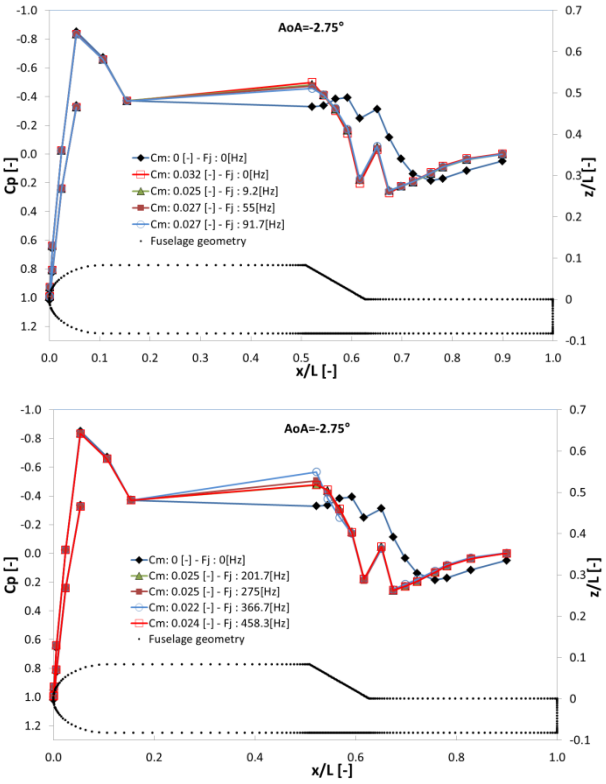

Figure 28: Pressure distribution for α=-5.5° varying the jet Frequency

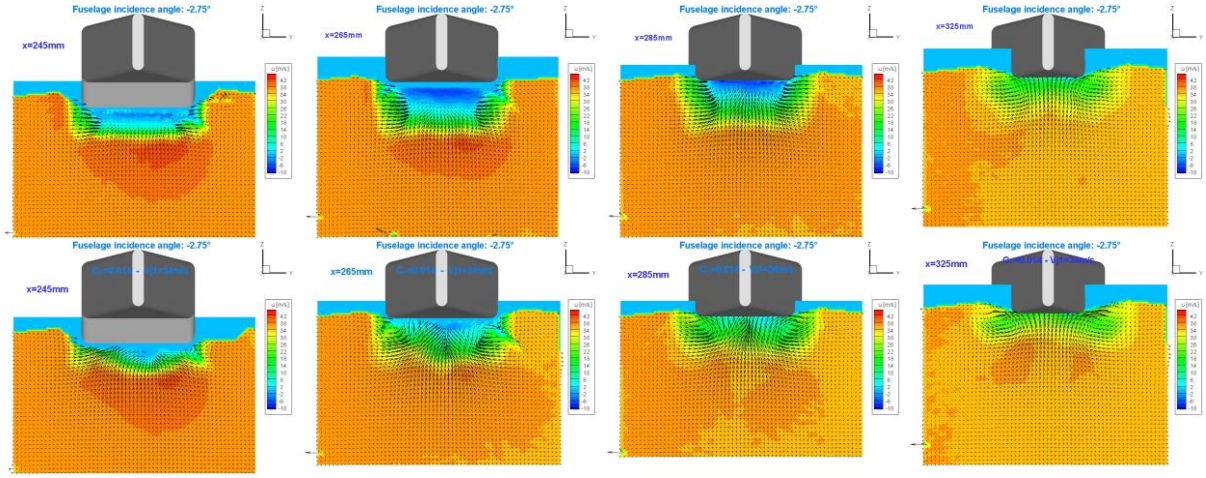

x/L=0.58 **x/L=0.63** **x/L=0.67** **x/L=0.77**

Figure 29: In plane velocity vectors and out of plane velocity contour map for the baseline (upper row) and for steady jet activated (lower row) at α=-2.75°

The effect of the steady jet on the three dimensional flow field in proximity of the fuselage bottom was well detailed by the stereo PIV results. The test cases characterized by the saturation values of the blowing coefficient were investigated for each single attitude angle. Only the operating configuration characterized by the single slot operating was investigated. The steady jet forced the flow reattachment beginning from the loading ramp reducing the eddy flow and altering also the vortex flow behavior moving a part from the centerline the two counter rotating vortices (Figure 29) with the double result to induce the pressure recovery on the ramp and reducing the suction on the cone tail moving the vortices away from the fuselage.

6. CONCLUSIONS

An experimental and numerical investigation of the flow characteristics behind the loading ramp of a simplified transport helicopter fuselage model has been carried out. Steady and pulsed jet actuators have been studied in order to reduce the pressure drag due to the typical eddy and/or vortex flows occurring in the wake region. Three different operating configurations were investigated for a wide range of blowing coefficient and reduced frequency. The following results have been reached:

1. The baseline model characterization has been obtained both experimentally by mean of WT test campaign and numerically by U-RANS simulation. The experiments indicate that the flow topology in the loading ramp region is mainly “vortex flow” type in the range between α=-11° to α=-5.5° and becomes “eddy flow” type for values larger than α=-2.75°. In between the two flow topologies cohabitates.
2. The preliminary CFD results indicate good agreement with the experiments for highly unsteady flow like the eddy flow when a minimum of 2000 time steps are computed. Less time steps are required in case of vortex flow.
3. The CFD simulations with AFC have not converged yet. The data validation shall be carried out in the future together with the evaluation of aerodynamic characteristics.
4. The test campaign clearly indicated that the configuration with a single slot provided the best pressure recovery at reduced cost in terms of blowing coefficient (more than 50%). The concurrence use of all slots blowing generated higher cost in terms of energy due to the jets interactions. Furthermore stronger vortex flow is induced by the side slots directed toward the model centerline.
5. For all the configurations a saturation value of the blowing coefficient was identified, which optimises the use of the actuators.
6. The single steady jet actuator induced pressure recovery on the loading ramp reducing the eddy flow and decreasing the undesired effect of the counter rotating vortices pushing them apart from the fuselage.
7. The pulsed jets tested were not able to influence the aerodynamic field with respect to the steady jets, neither they allowed to reduce the flow rate, due to the limited values of the velocity fluctuations achieved.
8. The test campaign was successful providing a better understanding of the rear loading ramp flow phenomena and especially the interaction with the selected actuators. The experimental database will be exploited for future CFD developments.
9. The results provided useful suggestion for the future planned industrial test campaign on the scaled 1:7 model of the AW101 transport helicopter. Some modifications shall be carried out to the rotating valve in order to increase the velocity fluctuation and reach the desired reduction of mass flow rate.
10. This paper does not discuss the cost of the flow control in terms of weight or power required for compressed air delivery. Obviously such a study would be platform dependent and is not part of the basic research.
11. In the future test campaign the exit angle of the side slots shall be modified and directed toward the external flow in order to prevent the formation of counter rotating vortices or push them outward.
12. Furthermore, in the next test campaign the effect of the side slots shall be evaluated for different yaw angle values.

ACKNOWLEDGEMENTS

The work has been partially founded by the European Union in the framework of the Clean Sky Project.

REFERENCE

[1] Gatard, J, Costes M, Kroll N, Renzoni P, Kokkalis A, Rocchetto A, Serr C, Larrey E, Filippone A, and Wehr D, High Reynolds Number Helicopter Fuselage Test in the ONERA F1 Pressurized Wind Tunnel, in 23rd European Rotorcraft Forum Paper 167, Dresden, Germany, September 16-18, 1997.

[2] Renaud T, Le Pape A, Pèron S, Numerical Analysis of Hub and Fuselage Drag Breakdown of a Helicopter Configuration in 38th European Rotorcraft Forum, Amsterdam, The Netherlands, September 4-7, 2012.

[3] Grawunder M, Reß, Breitsamter C, Adams NA, Flow Characteristics of a Helicopter Fuselage Configuration Including a Rotating Rotor Head, in 28th int. congress

of the aeronautical sciences, Brisbane, Australia, September 23-28, 2012.
[4] Ahmed, S.R.: Influence of base slant on the wake structure and drag of road vehicles. J. Fluids Eng. 105, 429–434 (1983)
[5] Seddon J, Basic helicopter aerodynamics. BSP Professional books, 1990, ISBN 0-632-02032-6
[6] Boniface J-C., A Computational Framework for Helicopter Fuselage Drag Reduction Using Vortex Generators, in proceedings of 70th American Helicopter Society, Montreal, Quebec, Canada, May 20-22, 2014
[7] Pahlke K, The GOAHEAD project, Proceedings of the 33rd European Rotorcraft Forum, Kazan, Russia, September 2007.
[8] Martin PB, Tung C, Hassan AA, Cerchie D, Roth J, Active Flow control Measurements and CFD on a transport Helicopter fuselage, in proceeding of 61st American Helicopter Society, 1-3 June, 2005.
[9] Eli Ben-Hamou, Eran Arad & Avi Seifert, Generic Transport Aft-body Drag Reduction using Active Flow Control, Flow Turbulence Combust (2007) 78:365–382, DOI 10.1007/s10494-007-9070-x.
[10] Schaeffler NW, Allan BG, Lienard C, Le Pape A, Progress Towards Fuselage Drag Reduction via Active Flow Control: A Combined CFD and Experimental Effort, presented at 36th European Rotorcraft Forum, Paris, September 7-9, 2010.
[11] Lienard C, Le Pape A, Verbeke C, Numerical and experimental Investigation of helicopter fuselage drag reduction using Active Flow Control, in 68th AHS Annual Forum, Fort Worth, TX, May 1-3, 2012.
[12] Le Pape A, Lienard C, Verbeke C, Pruvost M, De Coninck JL, Helicopter Fuselage Drag Reduction Using Active Flow Control: a Comprehensive Experimental investigation, in 69th AHS Annual Forum, Phoenix, Arizona, May 21–23, 2013.
[13] Crittenden T, Glezer A, Funk R, Parekh D (2001) Combustion-Driven Jet Actuators for Flow Control. AIAA Paper 2001-2768.
[14] George T. K. Woo, Ari Glezer, Jeremy Bain, and Lakshmi Sankar, Rotorcraft Fuselage Drag Reduction Using Combustion Powered Actuators, 49th AIAA Aerospace Sciences Meeting including the New Horizons Forum and Aerospace Exposition, Orlando, Florida, 4-7 January 2011.
[15] Woo GTK, Glezer A, Crittenden TM, Transitory Separation Control on a ROBIN Fuselage using Pulsed Actuation, in 37th ERF conference, Gallarate, Italy, 13-15 September, 2011.
[16] Martin PB, Overmeyer AD, Tanner PE, Wilson JS and Jenkins LN, Helicopter Fuselage Active Flow Control in the Presence of a Rotor, in proceedings of 70th American Helicopter Society, Montreal, Quebec, Canada, May 20-22, 2014.
[17] De Gregorio F, Helicopter fuselage drag reduction investigation, in proceedings of 17th International Symposium on Applications of Laser Techniques to Fluid Mechanics Lisbon, Portugal, 07-10 July, 2014.
[18] Menter F. R., Two Equation Eddy Viscosity Turbulence Models for Engineering Applications AIAA Journal, Vol. 32, No. 8, pp. 1598–1605 (1994).
[19] Kok, J. C., Resolving the dependence on free-stream values for the k-w turbulence model. AIAA J., Vol 38, No 7, 1292-1295 (2000).
[20] Spalart, P. R. and Allmaras, S. R., A One-Equation Turbulence Model for Aerodynamic Flows. AIAA Paper 92-0439 (1992).
[21] Marongiu, C., Catalano, P., Amato, M., and Iaccarino, G., U-ZEN: a computational tool solving U-RANS equations for industrial unsteady applications. 34th AIAA Fluid Dynamics Conference, Portland (Or), June 28-July 1 2004, AIAA Paper 2004-2345 (2004)
[22] Jameson, A., Time-Dependent Calculations Using Multigrid, with Application to Unsteady Flows Past Airfoils and Wings. AIAA Paper 91-1596 (1991)
[23] Turkel E., Preconditioning techniques in computational fluid dynamics. Ann. Rev. Fluid Mech. 31:385-416 (1999).
[24] Venkateswaran S., Buelow P. E. O., Merkle C. L., Development of linearized preconditioning methods for enhancing robustness and efficiency of Euler and Navier-Stokes Computations, AIAA Paper 97-2030 (1997).